Advanced Powder Technology xxx (xxxx) xxx

Contents lists available at ScienceDirect

Advanced Powder Technology

journal homepage: www.elsevier.com/locate/apt

Original Research Paper

Metallurgical slag properties as a support material for bimetallic nanoparticles and their use in the removal of malachite green dye

Alien Blanco-Flores [a,*], Helen P. Toledo-Jaldin [b], Alfredo R. Vilchis-Néstor [c], Gustavo López-Tellez [c], Víctor Sánchez-Mendieta [c], Delia M. Ávila-Márquez [d]

[a] División de Mecánica, Tecnológico de Estudios Superiores de Tianguistenco, Carretera Tenango-Marquesa Km 22, Santiago Tilapa, C.P. 52650 Santiago Tianguistenco, Estado de México, Mexico
[b] Facultad de Química, Universidad Autónoma del Estado de México, Paseo Colón y Tollocan s/n., C.P. 50000 Toluca, Estado de México, Mexico
[c] Centro Conjunto de Investigación en Química Sustentable UAEM-UNAM, Carretera Toluca, Atlacomulco Km 14.5, Unidad San Cayetano, C. P. 50200, Toluca, Estado de México, Mexico
[d] Instituto de Metalurgia-Facultad de Ingeniería, Universidad Autónoma de San Luis Potosí, Av. Sierra Leona 550, Lomas 2a sección, 78210 San Luis Potosí, San Luis Potosí, Mexico

ARTICLE INFO

Article history:
Received 18 March 2020
Received in revised form 6 May 2020
Accepted 11 May 2020
Available online xxxx

Keywords:
Steel slag
Fe-Cu nanoparticles
Chemical reduction method
Adsorption
Malachite green dye

ABSTRACT

Fe-Cu oxides nanoparticles (Nps) were embedded in two steel slag wastes (SSB and SSW) to develop SSB/Fe-Cu and SSW/Fe-Cu nanocomposites. Nps with mean sizes between 10–20 and 6–10 nm on SSW and SSB, respectively are agglomeration with a different shape. Their characteristics were investigated by XRD, TEM, BET, SEM techniques. The Nps modified the morphology of both support materials. XRD pointed out the presence of Cu and Fe. The proportion of Cu concentration was higher than the one of Fe. Nanocomposites were tested in malachite green removal from aqueous solution. The adsorption kinetic indicated physisorption and chemisorption as the main mechanisms of adsorption. The adsorption capacities were 88.26 and 63.55 mg/g for SSW/Fe-Cu and SSB/Fe-Cu, respectively. This novel, easy to prepare and low-cost nanocomposites is an efficient adsorbent material. The presence of calcium compounds may improve Nps deposition an MG removal. Materials with ferric phases are not as efficient as the first one; Fe is not well supported on the material. The removal of MG took place by dye structure modification and by interactions with Cu nanoparticles improving the oxidation-reduction process, through synergic effects.

1. Introduction

The population growth implies the increment of industrial activities: textile, leather, paper, and plastic, between others. It is estimated that over 15% of dyes world production is lost in the textile effluents. Besides, 128 tons of dyes are released daily into the environment worldwide [1]. This generates large volumes of colored wastewater, which are discharged in surface waters without treatment. As a consequence, the transmission of sunlight is inhibited and the photosynthesis activity is reduced destroying the ecosystem and aquatic life. Malachite green (MG) is a cationic dye, highly water-soluble. It is used as a coloring agent in textile, silk, and paper industries. It is a dermatological agent, biological stain in veterinary medicine, and dye for painting and printing inks. It is also applied widely as an antifungal, antibacterial, and anti-parasitical agent in cosmetics products [2]. MG is a highly persistent agent, carcinogenic, and teratogenic whose exposure may result in reproductive abnormalities in several fishes [3]. Jasińska *et al.*[4], reported that exposure to MG increases the risk of chromosomal fractures, reduces fertility, and may act as an inhibitor of respiratory enzymes. Therefore, the urgent removal of dyes from wastewater has attracted worldwide attention. Dyes are resistant to biological degradation therefore adsorption is an efficient, versatile, low cost, high efficient, simple, and easy operation process to remove toxic dyes [5]. The selection of efficient adsorbent material is associated with the number of surface groups, high surface area, pore size distribution, thermal stability, easy regeneration, reusability, disposal, and its abundance [6]. However, it is feasible to prepare materials functionalized with nanoparticles to obtained composites. The synergic effects caused by the combination of two or more materials may improve its capacity for the dye removal process. Nanotechnology is a novel technology that has attracted attention in the last decade. The use of Fe nanoparticles improves the removal of organic compounds, but the process is very slow. For this reason, several researchers have reported the addition of

* Corresponding author.
E-mail address: blancoflores81@hotmail.com (A. Blanco-Flores).

https://doi.org/10.1016/j.apt.2020.05.012
0921-8831/

a second metal such as copper (Cu) because the adsorption process might enhance compared to nanoscale iron alone [7].

The oxides of bimetallic nanoparticles have been used in several environmental applications as an effective adsorbent of dyes. Metal oxides in nanometric scale supported on the surface of another material are more effective due to the improvement of some properties [8]. Although various combinations of bimetallic oxides have been studied, only a few studies related to the Fe-Cu system for dyes removal in aqueous solutions have been reported. Besides, the presence of both oxides allows the process to take place in all ranges of pH [9,10]. The nanoparticles suffer the aggregation and this effect can be diminished through the immobilization of the nanoparticles inside different materials [11]. Waste, generated by several industries, is produced in huge quantities and most of them are finally placed without treatment. Without appropriate treatment, they can be considered as environmental passives that sooner or later generate polluting processes in the environment. For this reason, is important to develop new reuse methods; for example, in environmental applications such as adsorbent materials or nanoparticle material supports for removal of organic and inorganic compounds from wastewater [12].

During the production of one ton of steel 2–4 tons of steel, slag is produced, 35% of it is dumped as waste [13]. Its chemical composition normally consists of silicates, metallic and non-metallic oxides, sulfides, phosphates, iron, and aluminates. All these compounds are part of some mineralogical phases such as ferrites, which can influence pollutant removal from aqueous solutions [14]. Steel slag has been used for the building industry and treats acid mine drainage. However, its uses are conditioned to its quality since collateral reactions could occur during these applications.

40% of global steel production is produced in the electric arc furnace (EAF), where two types of slag can be found. The first one is known as *white slag*, it is a basic material obtained in the refining process which main compounds are calcium and magnesium oxides in more than 60%. The second one is a *black slag*, it is generated during melting scrap in the furnace whose main components are calcium, silicon, and iron oxides [15]. According to physicochemical and mineralogical characteristics, each type of steel slag has different behavior as support material of nanoparticles. They can benefit or not the removal of the dye but is necessary to study some aspects because of the lack of studies in this field.

This study aims to synthesize and characterize steel slag/Fe-Cu 95/5 wt% composite and to evaluate its adsorption properties to remove malachite green dye from aqueous solution. This study was carried out through the previous analyses of the effect and characteristics of different types of steel slag to support oxides Fe-Cu nanoparticles. The criterion of support material selection maximized the efficiency deposition of nanoparticles Fe-Cu.

2. Materials and methods

2.1. Steel slag

The steel slag (SS) white and black (SSW and SSB respectively) were obtained from "Antillana de Acero José Martí", Cuba, from

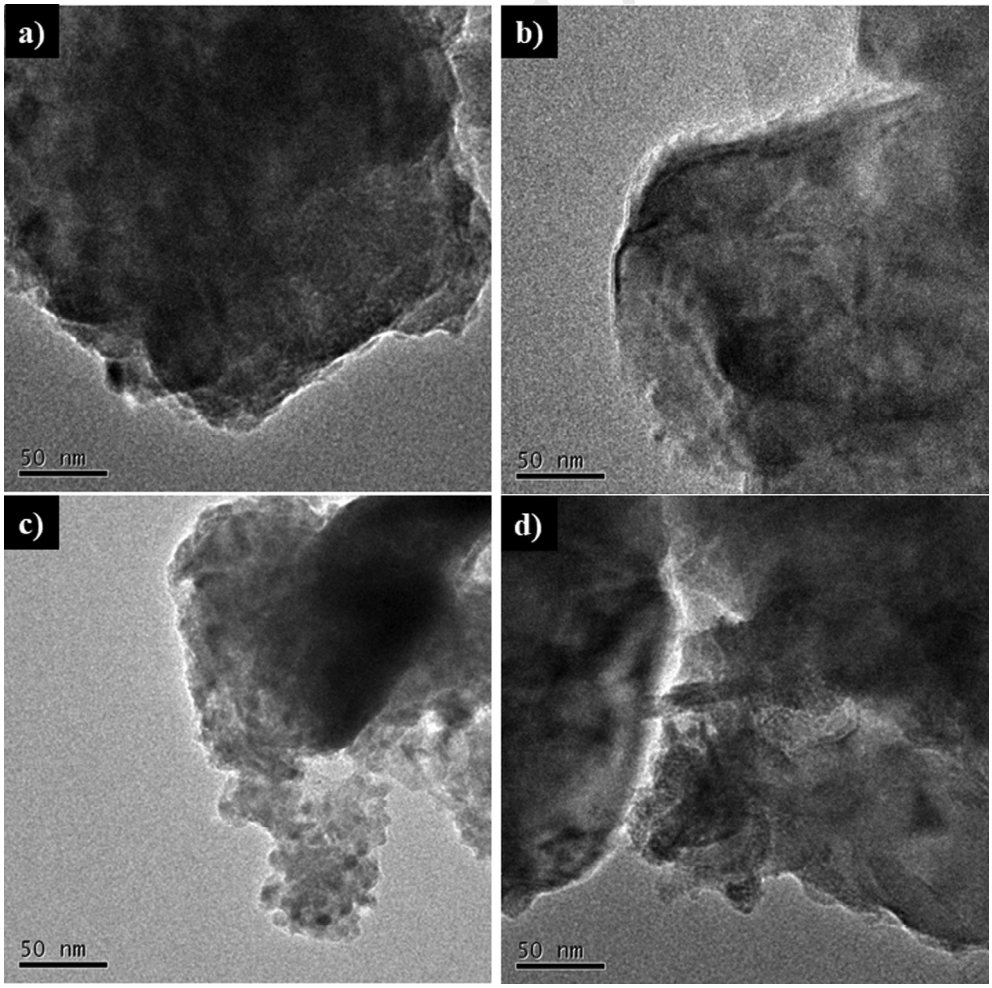

Fig. 1. TEM images of the Fe-Cu nanoparticles formed in the SSW/Fe-Cu (a-b) and SSB/Fe-Cu (c-d) nanocomposites.

Please cite this article as: A. Blanco-Flores, H. P. Toledo-Jaldin, A. R. Vilchis-Néstor et al., Metallurgical slag properties as a support material for bimetallic nanoparticles and their use in the removal of malachite green dye, Advanced Powder Technology, https://doi.org/10.1016/j.apt.2020.05.012

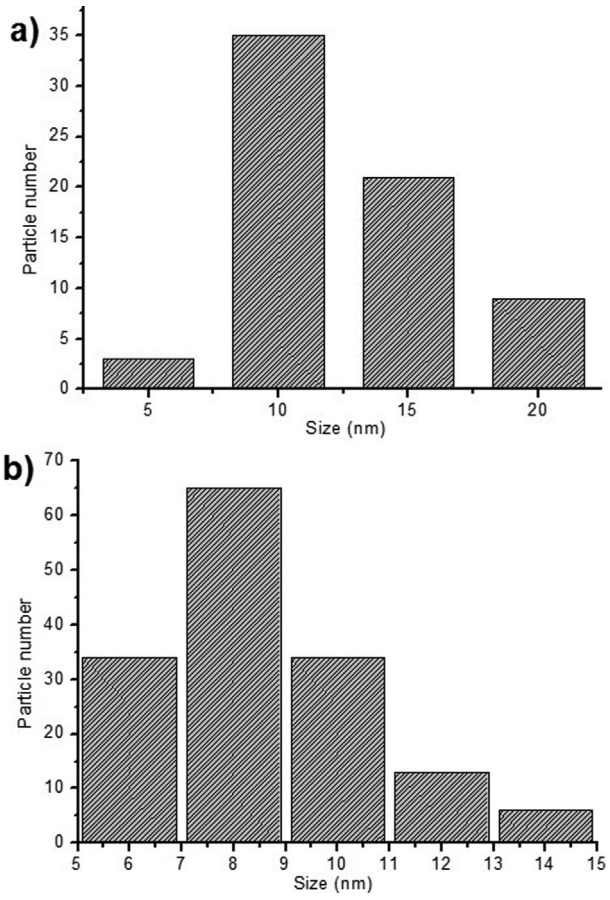

Fig. 2. Size of nanocomposite SSW/Fe-Cu (a) and SSB/Fe-Cu (b).

electrical arc furnace. The steel slag was crushed and sieved through 20 and 40-mesh. SS was washed with distilled water for 24 h, decanted, dried and stored for use in the synthesis of nanocomposites. Although solid waste presents ferric phases, these are fixed and engaged in the steel slag structure, and therefore the metallic ions do not interfere with the other phases.

2.2. Method of preparation of composites

The nanocomposites steel slag/Fe-Cu (SSW/Fe-Cu and SSB/Fe-Cu respectively) were synthesized using the reduction method reported in previous works. The ratio between Fe and Cu is 95/5 wt%. According a previews work [16] this rate is the best to mevoed the highest percentage of dye.

2.3. Characterization of composites

The surface morphology analyses of the nanocomposites were performed by scanning electron microscope (SEM) using a JEOL JSM-6510LV SEM microscope operated at 20 kV. Samples were fixed on a support with a carbon film and sputter-coated with gold to a thickness of ~ 200 Å. Transmission electron microscopy (TEM) observations were carried out using a JEOL 2100 microscope operated at 200 kV accelerating voltage. For TEM observations, the nanocomposites were dispersed by ultrasound in 2-propanol at room temperature (25 degreesC). A drop of the suspension was then placed on a carbon-coated Cu grid. To obtain statistically consistent information on the particle size distribution, the length of about 200 particles measuring, employing ImageJ™ software. The composites phase's analysis was investigated by X-ray powder diffraction (XRD) analysis. The XRD analysis was performed in a Bruker D8 Advance diffractometer with a Cu K_α radiation source operating at 30 kV and a tube current of 25 mA. XRD spectra were acquired with values of 2Θ from 5 to 80, with a step size of 0.03. The surface properties and surface area of the nanocomposites were characterized by N_2 adsorption measurements at 77 K using a surface area analyzer (Micromeritics Gemini 2360 instrument). The BET specific surface areas were determined by standard multipoint techniques of nitrogen adsorption. The determination of pore size was carried out by the method of BJH according to implemented software routines. X-ray photoelectron spectroscopy (XPS) was performed on an X Thermo Scientific model K-Alpha using Al Kα radiation (1486 eV) generated at 120 W. All binding energies were calibrated for the C1s peak (285 eV) arising from adventitious carbon. The spectra were analyzed using AVANTAGE, v4.87 software. The background subtraction was performed using the Shirley method; whenever curve fitting was needed the Gauss-Lorentz method was used.

2.4. Adsorbate

Dye solutions were prepared by dissolving an appropriate amount of dye in distilled water to obtain a range of concentrations corresponding to 30–120 $mg{\cdot}L^{-1}$ for successive dilutions. In this case, the basic dye malachite green chloride was used (CI = 42000, molecular formula: $C_{23}H_{25}N_2Cl$, pKa: 6.9, and molecular weight = 365 $g{\cdot}mol^{-1}$).

2.5. Adsorption experiments

The influence of the contact time over the amount of organic dye removal by the SSW/Fe-Cu and SSB/Fe-Cu nanocomposites was studied through batch experiments, at a dye initial concentration of 50 $mg{\cdot}L^{-1}$, adding 10 mL of dye solution to 10 mg of the nanocomposite. The mixture was shaken (120 rpm) at different times, and the adsorbent was separated by centrifugation. The experiments were performed in duplicate.

10 mg of nanocomposites were placed in contact with 10 mL at different initial concentrations of MG dye (30–120 $mg{\cdot}L^{-1}$) stirring during equilibrium time at room temperature. The mixture was centrifuged and decanted. The MG dye concentrations in the solutions were determined using a UV/Vis Perking Elmer Lambda 10 ultraviolet–visible spectrophotometer to 620 nm as maximum wavelength. The pH of each solution was measured before and after treatments. Kinetic and adsorption data of the adsorbed amount of dye at a time, q_t ($mg{\cdot}g^{-1}$ of adsorbent), were obtained by Eq. (1):

$$(C_o - C_t) \cdot V/m = q_t \quad (1)$$

Where, C_o ($mg{\cdot}L^{-1}$) is the initial dye concentration, C_t ($mg{\cdot}L^{-1}$) is the concentration of the solution at time t, V (mL) is the volume of treated solution, and m (g) is the mass of SSW/Fe-Cu and SSB/Fe-Cu nanocomposites.

The pH was not adjusted because of the importance of knowing the influence of nanocomposites without adding chemical compounds to maintain the pH stable. On the other hand, the proposed technology should be not only efficient but also cheap, and sustainable therefore the use of other chemicals could be counterproductive with these objectives.

Please cite this article as: A. Blanco-Flores, H. P. Toledo-Jaldin, A. R. Vilchis-Néstor et al., Metallurgical slag properties as a support material for bimetallic nanoparticles and their use in the removal of malachite green dye, Advanced Powder Technology, https://doi.org/10.1016/j.apt.2020.05.012

3. Results and discussion

3.1. Synthesis of nanocomposite

The nanocomposite is formed by steel slag, which is the matrix, and Fe/Cu nanoparticles or reinforcement. The nanocomposite can be synthesize because both phases are chemically stables. Bing et al., reported that the composition of slag is based on minerals (olivine, merwinite), RO (CaO–FeO–MnO–MgO solid solution), and free-CaO, between others. The only transformation that could happen is the volumetric expansion of CaO and MgO [17]. This transformation can favor the removal process because they are

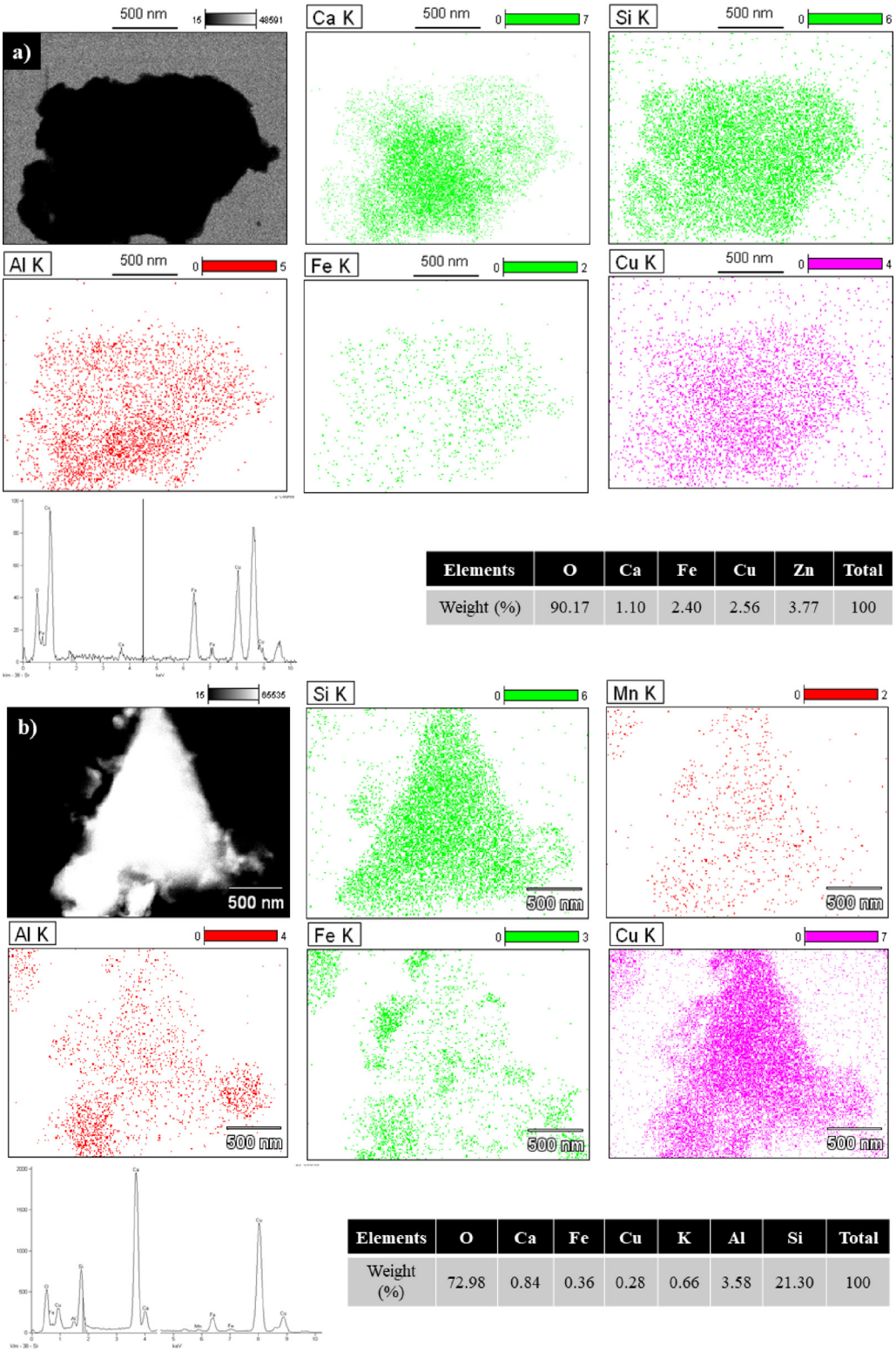

Elements	O	Ca	Fe	Cu	Zn	Total
Weight (%)	90.17	1.10	2.40	2.56	3.77	100

Elements	O	Ca	Fe	Cu	K	Al	Si	Total
Weight (%)	72.98	0.84	0.36	0.28	0.66	3.58	21.30	100

Fig. 3. EDS mapping of SSW/Fe-Cu (a) and SSB/Fe-Cu (b) nanocomposites. STEM – Bright and Dark Field micrographs are presented in figure a and b, respectively. Kα signal was employed to create the chemical mapping of Fe and Cu.

Please cite this article as: A. Blanco-Flores, H. P. Toledo-Jaldin, A. R. Vilchis-Néstor et al., Metallurgical slag properties as a support material for bimetallic nanoparticles and their use in the removal of malachite green dye, Advanced Powder Technology, https://doi.org/10.1016/j.apt.2020.05.012

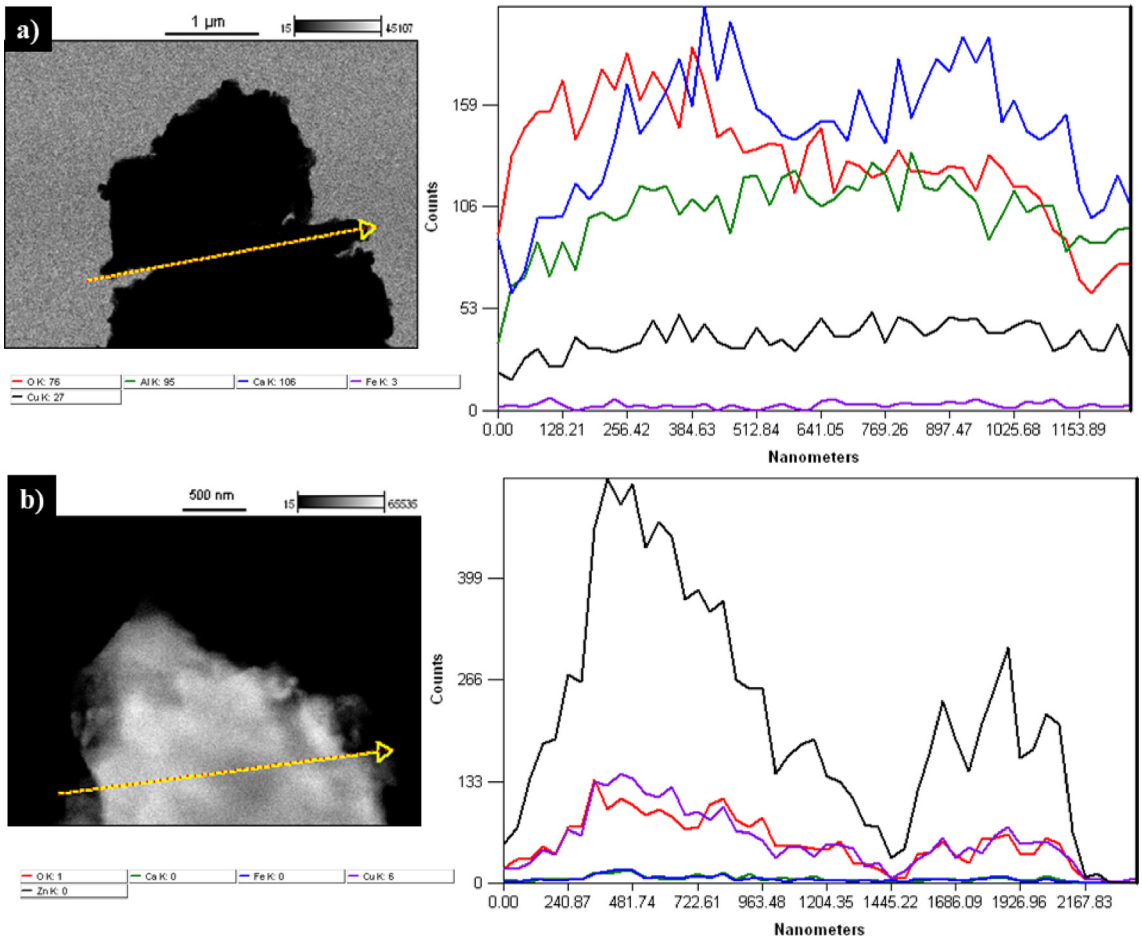

Fig. 4. STEM analysis of the SSW/Fe-Cu (a) and SSB/Fe-Cu (b) nanocomposites.

the primary responsible phases for organic and inorganic contaminants adsorption. It is known that Cu and Fe can better adhere to calcium phases [18], therefore through the XRD technique, it could be verified how these phases participate in the adsorption of nanoparticles on the surface of the slag.

The nanocomposite is considered thermally stable under the experimental conditions. Thermal stability was not an objective of the present research because the experiments were carried out at room temperature not exceeding 30 degrees. Steel slag and Fe/Cu alloys have high thermal stability reported by Eckert et al. [19]. Besides, steel slag is used as a Thermal insulator due to its high melting point, and non-combustible characteristic [20]. It is possible to work with both phases even at high temperatures above 100 degrees without decomposition of the material.

3.2. Characterization

TEM analyses confirmed the presence of nanoparticles on both supports (SSW and SSB). They are connected forming agglomerations as can be observed. They are spheroidal and few of them have an elongated form (Fig. 1 a-d). On SSB/Fe-Cu spheroidal and elongated nanoparticles are separated (Fig. 1 c-d) while on SSW/Fe-Cu they are mixed and therefore interconnected (Fig. 1 a-b). It can be inferred that the morphology of the support material could condition the shape of the nanoparticles and at the same time its distribution on the surface.

The size of nanoparticles oscillates between 10 and 15 nm and 6–10 nm for SSW/Fe-Cu and SSB/Fe-Cu respectively (Fig. 2 a-b). The difference between the sizes of nanoparticles is small due to the extent of surface area in both supports waste provided by size porous in both wastes. The value of its parameter in SSW was 0.941 m^2/g and 0.500 m^2/g for SSB. The surface area values in the supports are very similar, it was for this reason the small size of nanoparticles may be associated with the fast addition of reducing agent in the process of synthesis and its chemical composition [21]. Therefore, regardless of surface area, mineralogy and chemical composition of SSW and SSB the sizes of nanoparticles were similar, maybe influenced by the method of synthesis.

By EDS the presence of Fe and Cu elements was confirmed, while the chemical mapping collected from STEM mode showed homogeneous distributions of nanoparticles along on both support materials with slightly similar amounts of iron and copper (Fig. 3 a-b). The amount deposited on SSW was higher than on SSB, maybe because of the presence of several iron oxides in SSB which can block the active surface sites of deposition [22] or because of the ionic radius of copper is lower than of iron. It seems that copper has more affinity for being deposited in silicate phases (these phases is normally found in the highest amount in both types of slag), where the distribution of copper seems to cover a larger area of surface (Fig. 3 a-b).

The linear profile of the chemical composition of the SSW/Fe-Cu and SSB/Fe-Cu nanocomposites showed a mixture of both species in different proportions (Fig. 4 a-b). The intensity of the line pro-

Please cite this article as: A. Blanco-Flores, H. P. Toledo-Jaldin, A. R. Vilchis-Néstor et al., Metallurgical slag properties as a support material for bimetallic nanoparticles and their use in the removal of malachite green dye, Advanced Powder Technology, https://doi.org/10.1016/j.apt.2020.05.012

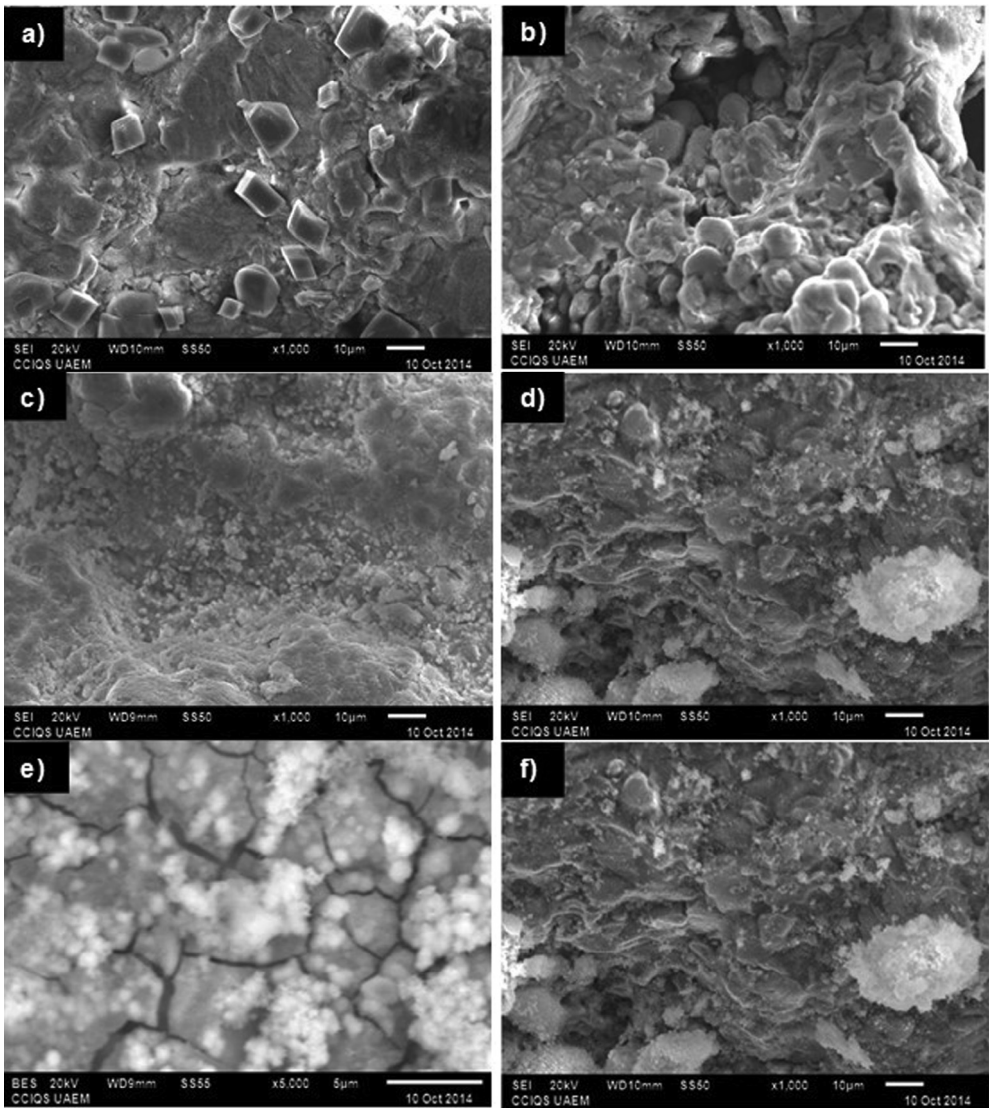

Fig. 5. SEM micrographs of SSW (a), SSB (b), SSW/Fe-Cu (c, e) and SSB/Fe-Cu (d, f) nanocomposites after malachite green dye adsorption.

files indicates the presence of copper in higher concentration in contrast with the iron even when the initial concentration of iron precursor was higher than copper. So, it seems that the mineralogical and chemical characteristics of both wastes do not favor the fixation of iron.

SEM micrograph of the solid wastes and nanocomposites can be observed in Fig. 5 a-f. Both surface change when nanoparticles were deposited (Fig. 5 a-b). SSW/Fe-Cu and SSB/Fe-Cu have a rough and heterogeneous surface, with particles agglomerated of different shape and size (Fig. 5 c-d). Differences between them were observed by the SEM micrograph. Each one has distinctive features; SSW/Fe-Cu present fractures in the surface, with little porosity development and quite smooth (Fig. 5 e). For SSB/Fe-Cu nanocomposite, the surface has completely contrary characteristics since the surface is rougher than SSW/Fe-Cu (Fig. 5 f). Textural characteristics may influence the adsorption process because the nanoparticles were fixed differently on both surfaces.

For the nanocomposites, the EDS analysis (Fig. 6 a-b) indicates a heterogeneous composition of alkaline, alkaline earth, and transition elements. In this case, the major element is oxygen, followed by iron, copper, and calcium for SSW/Fe-Cu and silicon, iron, and calcium for SSB/Fe-Cu. EDS confirms the results obtained by EDS-TEM; more copper than iron was fixed in both wastes.

The XRD results showed the presence of several phases of basic wastes, iron, and copper oxide nanoparticles. The latter is mixed with corresponding phases of wastes (Fig. 7 a-b). In SSW/Fe-Cu appeared phases related to Cu but SSB/Fe-Cu showed more phases related to Fe than to Cu. These results are consistent with the results obtained by SEM, TEM, and STEM techniques.

The calculated BET surface for SSW/Fe-Cu was 0.213 m^2/g. The surface area for SSW was higher than for its nanocomposite ($S_{eBET,(SSW)}$ = 0.941 m^2/g). Also, the average pore size diameter for SSW/Fe-Cu increase (D_d = 5.678 nm and D_{pSSW} = 3.854 nm). This result might indicate the appearance of new mesopores due to a rapid aggregation of Fe-Cu nanoparticles [22]. The surface area for SSB/Fe-Cu was 1.627 m^2/g, which was higher than for SSB ($S_{eBET,(SSB)}$ = 0.500 m^2/g). For nanocomposite, D_p decrease comparing with the value of waste SSB ($D_{pSSB/Fe-Cu}$ = 1.43 nm and D_{pSSB} = 3.850 nm), because the pore formed might be lower. Although the values of this parameter in the nanocomposites are low, the presence of nanoparticles supported in both wastes could contribute to enhancing of MG removal. All results are in concor-

Please cite this article as: A. Blanco-Flores, H. P. Toledo-Jaldin, A. R. Vilchis-Néstor et al., Metallurgical slag properties as a support material for bimetallic nanoparticles and their use in the removal of malachite green dye, Advanced Powder Technology, https://doi.org/10.1016/j.apt.2020.05.012

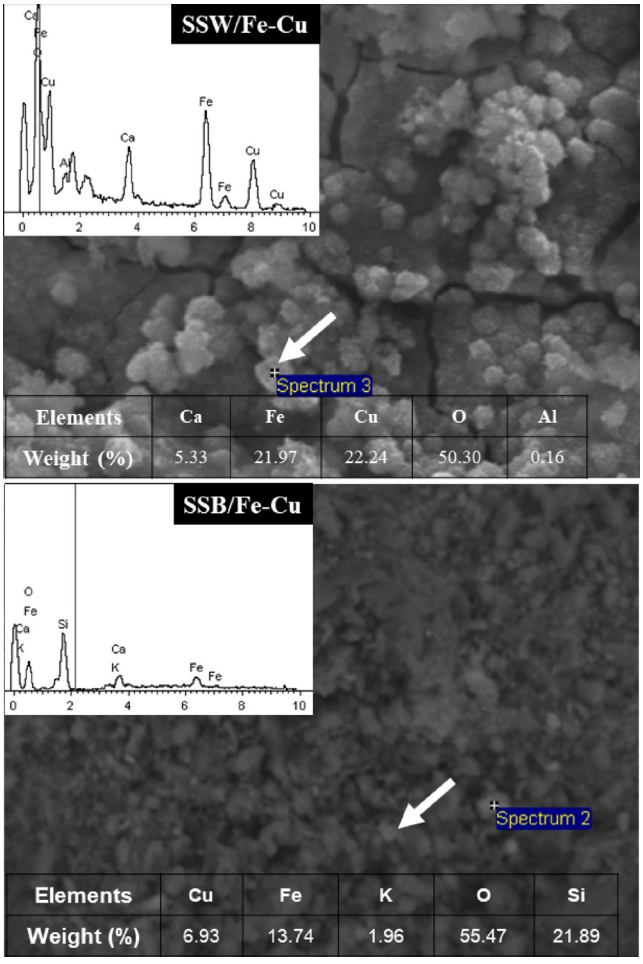

Fig. 6. EDS-SEM micrographs of SSW/Fe-Cu (a) and SSB/Fe-Cu (b) nanocomposites after malachite green dye adsorption. (For interpretation of the references to colour in this figure legend, the reader is referred to the web version of this article.)

dance with surface observed by SEM with large particles agglomerates and low development of pores.

Therefore, the SSW waste had more affinity fort Fe-Cu oxide nanoparticles and SSB showed a lower affinity for Cu oxide nanoparticles. The difference between the two wastes can be explained regarded their morphological surface and chemical and mineralogical composition, where the support enrichment, in basic phase, presents more affinity for this bimetallic nanoparticles system.

3.3. Kinetics adsorption

The results reveal that the adsorption process was slower for SSW/Fe-Cu, while SSB/Fe-Cu removed more in less time (Fig. 8 a-b). Pourjavadi *et al.*, [23] consider that rapid adsorption is associated with an abundance of adsorption active sites on the adsorbent surface in the initial stage of the contact. In this regard, it is possible that the SSB/Fe-Cu offer more active adsorption sites than SSW/Fe-Cu or that the nanoparticles supported on SSB waste are more efficient than on SSW waste. Therefore, the incorporation of nanoparticles modified the process velocity in both support materials.

The equilibrium time was reached at 260 min and 125 min for SSW/Fe-Cu and SSB/Fe-Cu, respectively. The process was twice slower for SSW/Fe-Cu nanocomposite than for SSB/Fe-Cu. It seems that the incorporation of Fe-Cu oxide nanoparticles in SSW interferes in the diffusion process, making the access to surface active sites more difficult, maybe by aggregation of nanoparticles onto the surface of SSW. In SSB waste, the minor presence of Cu oxide nanoparticles supported or surface morphology of nanocomposite can decrease the time to achieve the greater adsorption or improve the mobility of dye molecules to the active adsorption sites.

The pseudo-first and pseudo-second-order kinetic models were selected for the kinetic data analysis based on a previous nanocomposite characterization. They have different morphology as a result of nanoparticles aggregations and the presence of steel slag characteristic phases. This implies that the adsorption processes may happen between the dye molecule and the nanocomposites by different ways, therefore the mentioned models are those that describe a chemical and physical adsorption processes. Therefore, pseudo-first, pseudo-second, and second-order kinetic models [24] were used to obtain information about the mechanism of the adsorption.

The kinetic process was better described by pseudo-first and pseudo-second-order model for SSW/Fe-Cu and SSB/Fe-Cu, respectively (Table 1). This suggests that the removal of malachite green dye with the two nanocomposites was carried out by the different processes. For the first one, the process was described through the physisorption process, and in the latter nanocomposite, this was described by chemisorption. Nevertheless, we cannot rule out that chemical adsorption process because it can occur simultaneously according to values of correlation coefficient (R^2) obtained for SSB/Fe-Cu nanocomposite: physisorption and chemisorption.

In the case of SSW/Fe-Cu, the value of pseudo-first-rate constant decreases compared to SSB/Fe-Cu ($k_{1SSW/Fe\text{-}Cu} = 0.009\ min^{-1}$ and $k_{1SSB/Fe\text{-}Cu} = 0.058\ min^{-1}$). So that the nanoparticles supported have influence over the rate adsorption of MG dye for both nanocomposites in a different way.

The adsorption involved multi-step related to diffusion and mass transport process. To corroborate the rate-controlling step, the intraparticle diffusion model [25] was applied:

$$q_t = k_i t^{1/2} + C \quad (1)$$

where k_i is the intraparticle diffusion rate constant, C indicates the thickness of the boundary layer and external mass transfer resistance.

The plot for both nanocomposites is multilinear and these lines do not pass through the origin, thus it may indicate that not only intraparticle diffusion but also the film diffusion (boundary layer) are the rate-controlling step [26] (Fig. 9 a and b). The slope and intercept of the lines provide information about k_i and C. In this respect, the constant C increased from SSW/Fe-Cu to SSB/Fe-Cu. This behavior is related to the increase of thickness of the boundary layer and increase of the external mass transfer resistance while the internal mass transfer must be favored. The results obtained from k_i support previous results. Therefore, it was expected that SSB/Fe-Cu nanocomposite removes a greater amount of dye. However, comparing the values of adsorption and desorption constant (a and b, respectively) derived of the second-order kinetic model (Table 1) for SSB/Fe-Cu nanocomposite, it has a greater tendency to desorb than the affinity to adsorb the dye even when the diffusion process is favored in SSB/Fe-Cu nanocomposite.

3.4. Adsorption isotherm

Several models have been developed to describe the behavior of adsorbent materials. In this investigation, Langmuir, Freundlich, Langmuir-Freundlich, and Temkin adsorption isotherm models were applied [27] (Fig. 10).

Please cite this article as: A. Blanco-Flores, H. P. Toledo-Jaldin, A. R. Vilchis-Néstor et al., Metallurgical slag properties as a support material for bimetallic nanoparticles and their use in the removal of malachite green dye, Advanced Powder Technology, https://doi.org/10.1016/j.apt.2020.05.012

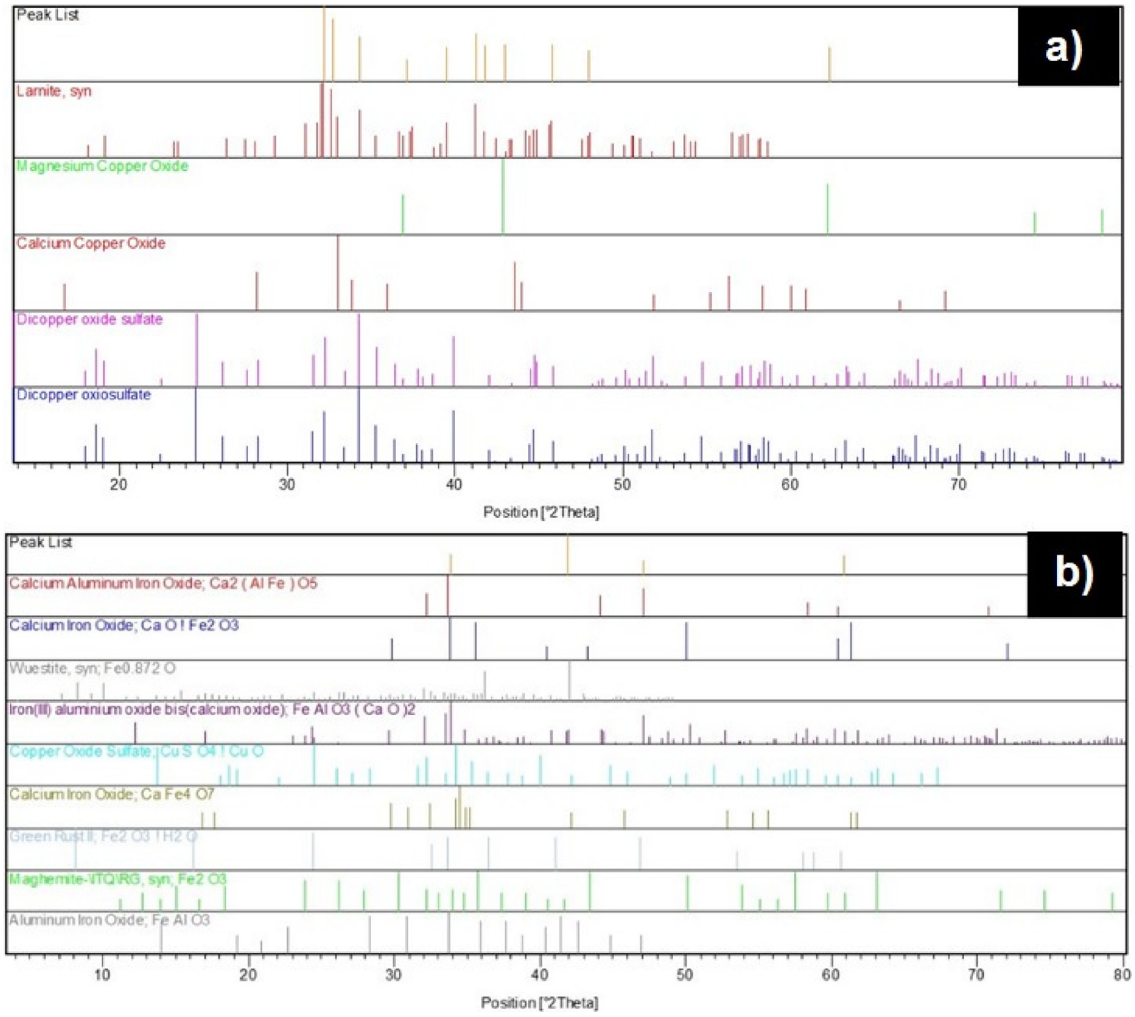

Fig. 7. XRD analysis of the SSW/Fe-Cu (a) and SSB/Fe-Cu (b) nanocomposites.

The maximum adsorption capacity of the nanocomposites was found to be 88.26 and 63.55 mg/g for SSW/Fe-Cu and SSB/Fe-Cu, respectively (Table 2). Langmuir isotherm model provides the best R^2 for experimental data for SSW/Fe-Cu and Langmuir-Freundlich for SSB/Fe-Cu nanocomposite. In this sense, the higher adsorption was achieved with the first nanocomposite (SSW/Fe-Cu). In this case, the adsorption takes place at specific homogeneous and uniform site surfaces. Whereas for SSB/Fe-Cu the adsorption was better described for the Langmuir-Freundlich model that described the adsorption process through the heterogeneous surface where occur different or a combination of many processes. Therefore, the adsorption removal was higher with material where Cu oxides nanoparticles were deposited to a major extent (SSW/Fe-Cu). Analyzing the Langmuir constant (K_L), related to the interaction between adsorbent-adsorbate [28], the nanocomposite SSB/Fe-Cu had a greater interaction with MG molecules despite the other nanocomposite. The amount of Cu oxide nanoparticles maybe determine not only the amount of dye removed but also the strength of the interaction between adsorbate and adsorbent. In this sense, those supports with high iron content (SSB/Fe-Cu) will have greater interactions with malachite green molecules that nonferrous supports with iron and copper supported therein (SSW/Fe-Cu).

Freundlich constant (K_F) indicates the extent of adsorption, this assumes that the more extent of the process takes place using the SSW/Fe-Cu nanocomposite; also, this is nanocomposite that most adsorbed MG dye. 1/n is the heterogeneity factor for a range between 0 and 1. If the value is close to 0 then it is more than heterogeneous surfaces [29], Therefore SSB/Fe-Cu (0.09) showed a more heterogeneity surface than SSW/Fe-Cu (0.13), which matches the best model adjusted to experimental data of SSB/Fe-Cu nanocomposite.

The heat adsorption was higher for SSB/Fe-Cu (15.53 $J \cdot mol^{-1}$) than SSW/Fe-Cu (9.94 $J \cdot mol^{-1}$). This parameter is likely related to the heterogeneity surface because it matches the behavior for the 1/n parameter.

The experimental conditions of the adsorption process do not imply aggressive conditions. A potential degradation of the chemical phases was avoided since the process took place at room temperature, and in an aqueous medium where the contact time is very short. Diffusive processes of the ions that form the stable chemical phases of the material is not possible. In a previous work, steel slag and nanoparticles in aqueous solution were analyzed in order to establish a potential chemical elements desorption. The analysis established that under these conditions there is no chemical elements desorption or degradation [30].

Analyzing the results, it can also be inferred that both, support materials and nanoparticles influenced the effectiveness of the adsorption process. The greatest removal was achieved with the solid waste nonferrous that had more copper-deposited (SSW) in its surface.

Venkata et al., [31] reported that the surface properties play an important role in numerous important technologies. X-ray photoelectron spectroscopy (XPS) is a widely used method for surface

Please cite this article as: A. Blanco-Flores, H. P. Toledo-Jaldin, A. R. Vilchis-Néstor et al., Metallurgical slag properties as a support material for bimetallic nanoparticles and their use in the removal of malachite green dye, Advanced Powder Technology, https://doi.org/10.1016/j.apt.2020.05.012

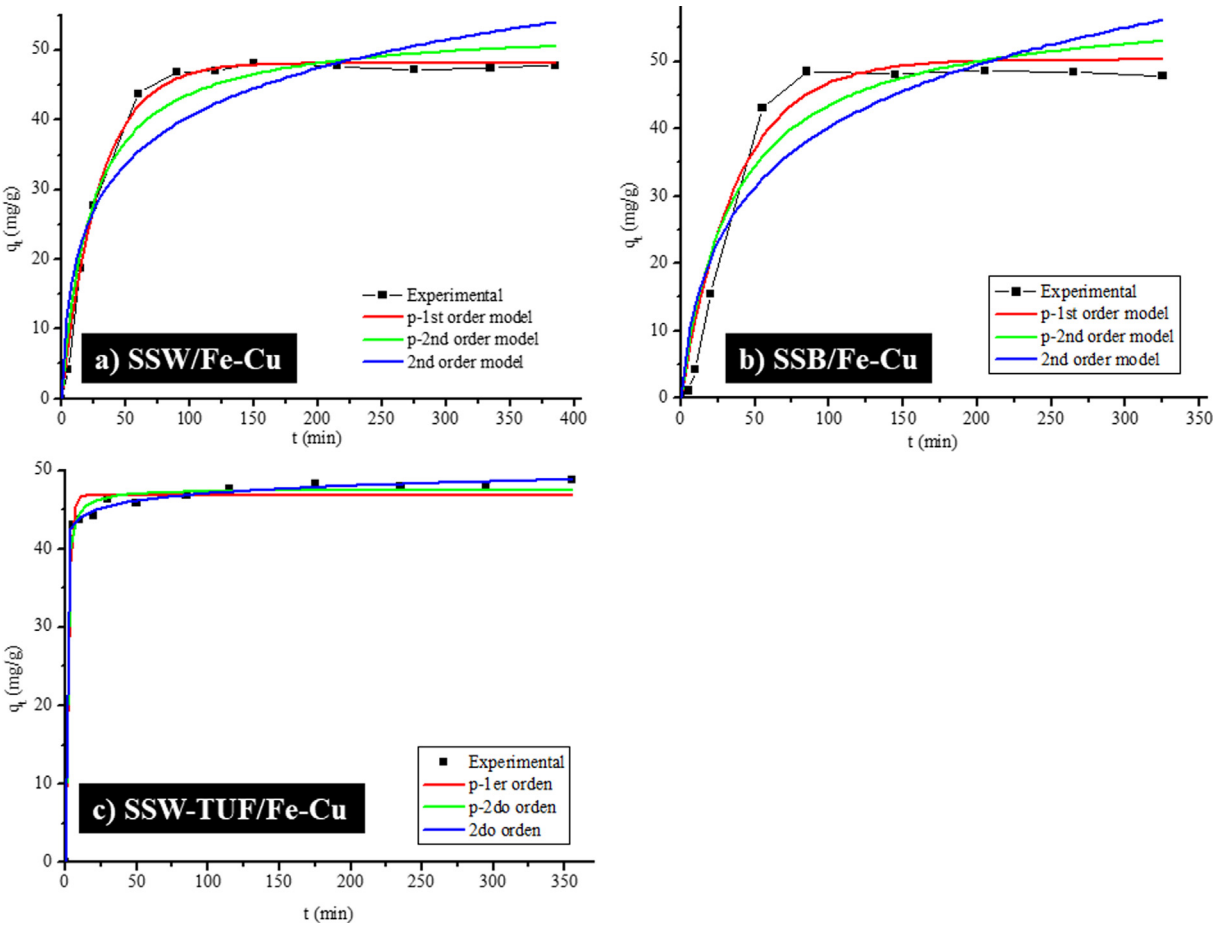

Fig. 8. Adsorption kinetics plots of SSW/Fe-Cu (a), SSW/Fe-Cu (b) and SSW-TUF/Fe-Cu (c) for MG removal with the nanocomposites.

Table 1
Kinetic parameters for the adsorption process of MG dye on nanocomposites.

Parameters	SSW/Fe-Cu q_{eexp} = 48.68 mg/g	SSB/Fe-Cu q_{eexp} = 47.45 mg/g	SSW-TUF/Fe-Cu q_{eexp} = 47.61 mg/g
Pseudo first order model			
q_{ecal} (mg/g)	54.06	47.08	46.88
k_1 (min^-)	0.009	0.58	0.47
R^2	0.9851	0.9964	0.9862
Pseudo second order model			
q_{ecal} (mg/g)	75.75	47.49	47.66
K_2 (g/mg·min)	$6.6 \cdot 10^{-5}$	0.056	0.030
R^2	0.9775	0.9999	0.9947
Second order model			
a (mg/g)	0.58	2.50	1.18
b (mg/g)	0.040	1.55	0.73
R^2	0.9689	0.9996	0.9989
Intraparticle diffusion model			
k_i (g/mg·$min^{1/2}$)	4.41	0.064	0.54
C	12.01	46.41	41.93
R^2	0.9652	0.8839	0.9954

analysis of materials, due to its surface sensitivity and chemical specificity. Therefore, these results were confirmed through XPS analyses for nanoparticles without support. In this case, was found that copper play an important role in dye removal.

To examine the presence of Fe-Cu elements in the nanoparticles synthesized, X-ray photoelectron spectra (XPS) measurements were realized. The results obtained correspond to the aforementioned Fe, Cu, and O elements, confirming the presence of these metal elements as oxides. Peaks at 2p3/2 y 2p1/2 region confirm the presence of Fe and Cu [32] (Table 3).

The region corresponding to the binding energy of Cu 2p3/2 signal was deconvoluted taking into account the respective FWHM [33]. For Cu 2p3/2 spectrum, the peaks at 932.63, 933.6, 934.3, and 935.3 eV are related to Cu(I)FeO_2 or Cu^0, Cu_2O, Cu(OH) and CuO respectively. The Fe 2p3/2 peak at 711 eV is associated with Fe_2O_3 species also appear a peak at 713.3 eV, which would correspond, to the interaction between Fe, Cu, and O [34].

After MG was adsorbed, some signals were shifted and others disappeared due to the interaction between the dye molecules and surface groups. Cu2p3/2 only observed signals at 932.5 eV related to Cu(I), FeO_2 or Cu^0. The hypothesis is that the dye was oxidized when Cu^{2+} species were reduced. In the Fe 2p3/2 region, there are peaks at 710.4 and 712.4 eV assigned to FeO and α-FeOOH respectively. Analyzing the last one noted a shift from 713.3 eV (before MG adsorbed) to 712.4 eV (after MG adsorbed). This behavior could be caused by Cu reduction to dye oxidize and therefore the interaction Fe-Cu-O can disappear. The aforementioned is possible to corroborate using redox potential of Cu^{2+}/Cu and Fe^{2+}/Fe, which are 0.34 V and −0.44 V, respectively. In this sense, is easier to reduce Cu^{2+} than Fe^{2+}. It is also possible that Fe^{3+} (as Fe_2O_3) could be reduced to Fe^{2+} (as FeO) because the redox potential is more positive (0.77 V) and thus the FeOOH is formed, considering that the removal process occurred in aqueous solution.

Please cite this article as: A. Blanco-Flores, H. P. Toledo-Jaldin, A. R. Vilchis-Néstor et al., Metallurgical slag properties as a support material for bimetallic nanoparticles and their use in the removal of malachite green dye, Advanced Powder Technology, https://doi.org/10.1016/j.apt.2020.05.012

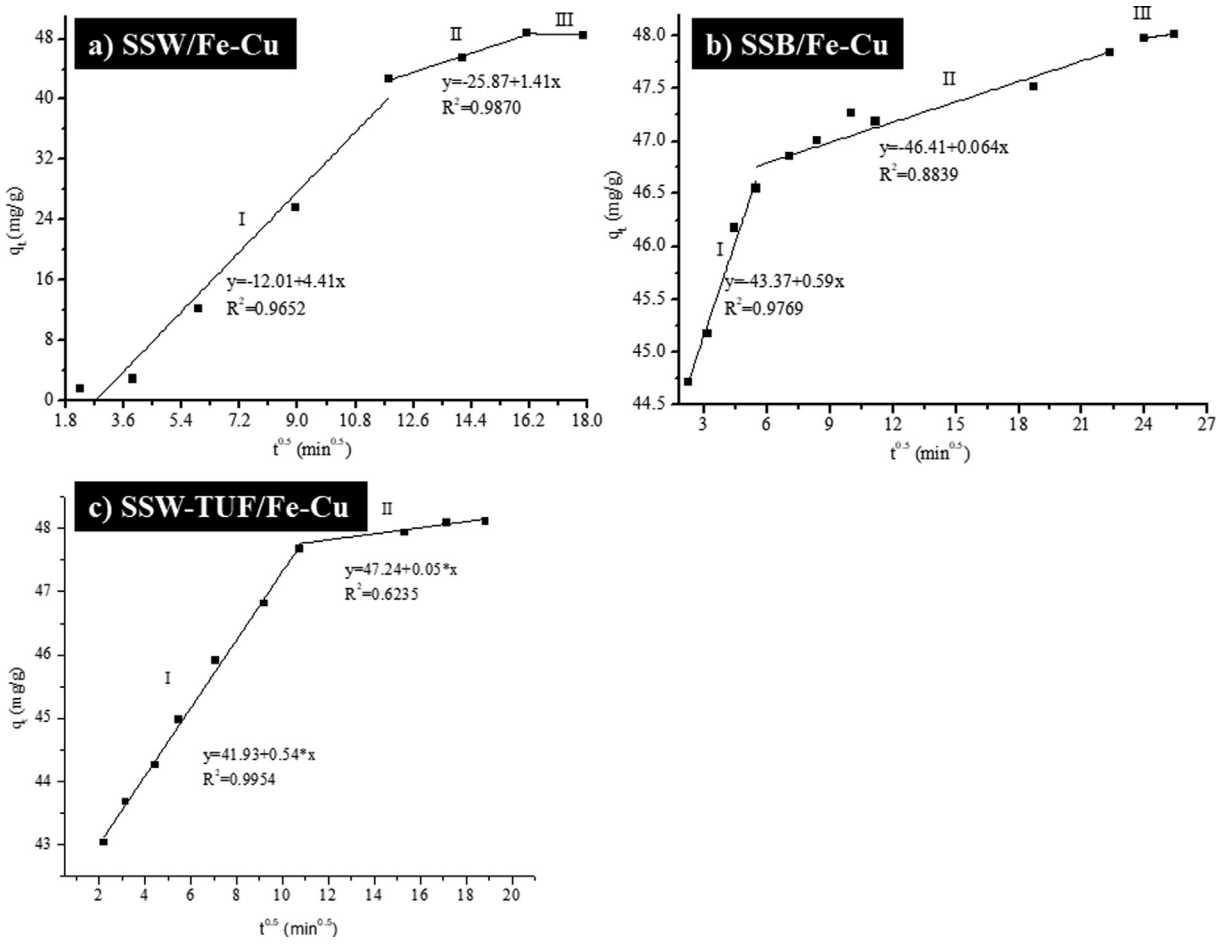

Fig. 9. Intraparticle diffusion plots for SSB/Fe-Cu (a), SSW/Fe-Cu (b) and SSW-TUF/Fe-Cu (c) nanocomposites.

There are two peaks at 396.5 and 402.9 eV in the XPS spectra of N1s, which are related to tertiary nitrogen and quaternary amine. Also although the first signal presents a shift probably associated with the chemical environment of an aromatic ring or the interaction between Cu species and the transformation of MG structure in leucomalachite dye. This is confirmed by analyzing the three O signals: 530.22, 529.88 y 532.26 eV corresponding to FeOOH, FeO, and OH-malachite green carbinol, respectively (Table 3).

Serpil et al., refer to the affinity that nitrogen atoms exhibit toward Cu^{2+} sorption [35]. In this case, the removal was carried out through interaction between Cu nanoparticles and dye molecules. The MG dye has amine groups as functional groups. Amines have a pair of electrons that can interact specifically with copper ions because it behaves as a Lewis acid and also has its 3d orbit incomplete; therefore, copper ions can coordinate and form complexes with a Lewis base such as the amines. The removal of dye by SSW/Fe-Cu nanocomposite also supports because the pH of solutions is basic due to the presence of calcite and magnesium phases. Thus, the MG dye changes to the resonant form and promote the others process such as hydrogen bond or exchange ions (Fig. 11).

To verify that the calcium phases benefit the removal of the dye, a material of the same nanoparticle system was formed. White slag and a calcium mineral known as tuffite (TUF) were reported by Blanco-Flores *et al.,* [36]. In this case, the white slag (SSB) was mixed in a 3: 1 ratio with the calcium mineral, and on this new material Fe-Cu nanoparticle was supported. The adsorption kinetic adjustment changes to the Elovich model and also the shape of the graph was different, so does the equilibrium time (115 min) indicating that the adsorption was faster in the early stages. The dye removal was a chemical process in a heterogeneous surface (Fig. 8 c, table 1). When the diffusion mechanism was analyzed, it was evident in Fig. 9c that the diffusion was faster than in the other two cases. This may be because the incorporated mineral has a texture that favors the diffusion into adsorption sites. The adsorption capacity increased up to three times for this new compound (267.09 mg / g) exceeding the capacity of SSW / Fe-Cu and SSB / Fe-Cu (Table 2). However, the value of adsorption obtained by the tuffite composite was lower (TUF/Fe-Cu, q_m = 376.66 mg/g) according to Blanco-Flores et al., [16].

The values of adsorption capacity were compared with various adsorbent materials (Table 4) considering the experimental conditions. The adsorption capacity of the nanocomposites was greater than the rest. The comparison showed that SSW/Fe-Cu nanocomposite has a large adsorption capacity followed SSB/Fe-Cu. Therefore, SSW/Fe-Cu and SSB/Fe-Cu are potentially adsorbent materials for wastewater treatment.

The steel slag disadvantage is the volume expansion, CaO and MgO react with water to form calcium and magnesium hydroxides. Therefore, the material required a pretreatment to inactive these

Please cite this article as: A. Blanco-Flores, H. P. Toledo-Jaldin, A. R. Vilchis-Néstor et al., Metallurgical slag properties as a support material for bimetallic nanoparticles and their use in the removal of malachite green dye, Advanced Powder Technology, https://doi.org/10.1016/j.apt.2020.05.012

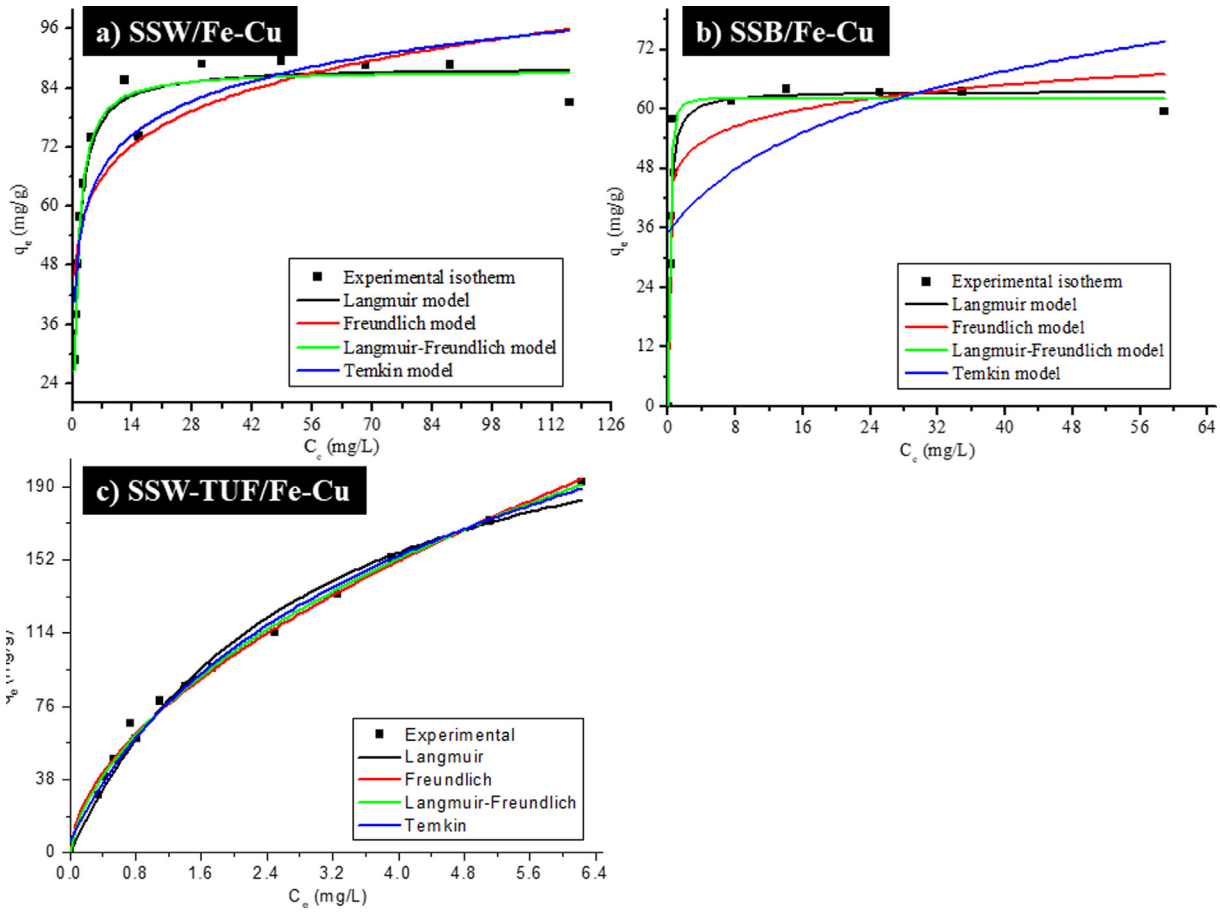

Fig. 10. Adsorption isotherms of SSW/Fe-Cu (a), SSB/Fe-Cu (b) and SSW-TUF/Fe-Cu (c) nanocomposites for MG removal.

Table 2
Isotherm parameters for MG dye adsorption.

Parameters	SSW/Fe-Cu	SSB/Fe-Cu	SSW-TUF/Fe-Cu
Langmuir model			
q_m (mg/g)	88.26	63.55	267.09
K_L (L/mg)	1.02	5.09	0.35
R^2	0.9604	0.9373	0.9862
Freundlich model			
k_F (mg/g)	51.02	47.36	69.70
1/n	0.13	0.09	0.56
R^2	0.7464	0.8614	0.9937
Langmuir-Freundlich model			
q_m (mg/g)	87.40	14.61	77.12
K_{FL} (L/mg)	1.26	9.08	0.11
1/n	0.91	1.96	0.66
R^2	0.9600	0.9477	0.9940
Temkin model			
A (L/mg)	1.29	7.38	1.06
B (J/mol)	9.94	15.53	95.08
R^2	0.8182	0.3166	0.9919

phases. This pre-treatment consumes a lot of energy and time to achieve below 0.5% of volume instability [37]. The present research considers the inactivation of those phases by the interaction with Fe, Cu, and malachite green dye. This process can be verified by XRD results (Fig. 7).

After dye adsorption, the material can return to building industries and uses as road pavement constructions or aggregate in constructions involving concrete. This application is the target of another investigation which will be published soon.

4. Conclusion

Preparation of novel SSW/Fe-Cu and SSB/Fe-Cu nanocomposites was achieved by a simple and inexpensive chemical reduction method. SEM, TEM, XRD, and BET results indicated the presence of Fe-Cu oxides nanoparticles supported or embedded in both wastes. Fe-Cu agglomeration of nanoparticles with different shapes and sizes between 10 and 20 and 6 and 10 nm on SSW and SSB were established by characterization technics. Also, the nanoparticles modified the morphology of both wastes. XRD showed the presence of several phases related to Cu and Fe species. In the composites, the Cu moieties concentration was higher than those of Fe. SSW/Fe-Cu nanocomposite removed MG dye from aqueous solutions in an efficient way. The adsorption kinetics of MG on these nanocomposites was better described by pseudo-first and pseudo-second-order model for SSW/Fe-Cu and SSB/Fe-Cu, respectively. Therefore, the adsorption process, for the former nanocomposite, takes place at specific homogeneous and uniform sites surface. The removal of dye with SSB/Fe-Cu was carried out through a combination of many processes. The adsorption capacity was 88.26 and 63.55 mg/g for SSW/Fe-Cu and SSB/Fe-Cu respectively. The best removal was achieved with the support material having calcium phases, where nanoparticles were better supported. The dye exhibited more affinity for Cu than for Fe nanoparticles. The removal was carried out through interaction between Cu

Please cite this article as: A. Blanco-Flores, H. P. Toledo-Jaldin, A. R. Vilchis-Néstor et al., Metallurgical slag properties as a support material for bimetallic nanoparticles and their use in the removal of malachite green dye, Advanced Powder Technology, https://doi.org/10.1016/j.apt.2020.05.012

Table 3
Binding energies (eV) from XPS spectra for SSW/Fe-Cu before and after MG dye removal.

Samples	Species	$Cu2p^{3/2}$	$Fe2p^{3/2}$	O1s	N1s
SSW/Fe-Cu	$Cu(I)FeO_2$ or Cu^0	932.63	–	–	–
	Cu_2O	933.6	–	–	–
	Cu(OH)	934.3	–	–	–
	CuO	935.3	–	–	–
	Fe_2O_3	–	711	–	–
	$Cu(I)FeO_2$	–	713.3	–	–
SSW/Fe-Cu-dye	$Cu(I)FeO_2$ or Cu^0	932.5	–	–	–
	FeO	–	710.4	–	–
	α-FeOOH	–	712.4	–	–
	$-N(CH_3)_2$	–	–	–	396.5
	$=N(CH_3)_2$	–	–	–	402.9
	FeOOH, y	–	–	530.2	–
	FeO	–	–	529.8	–
	OH-malachite green carbinol	–	–	532.2	–

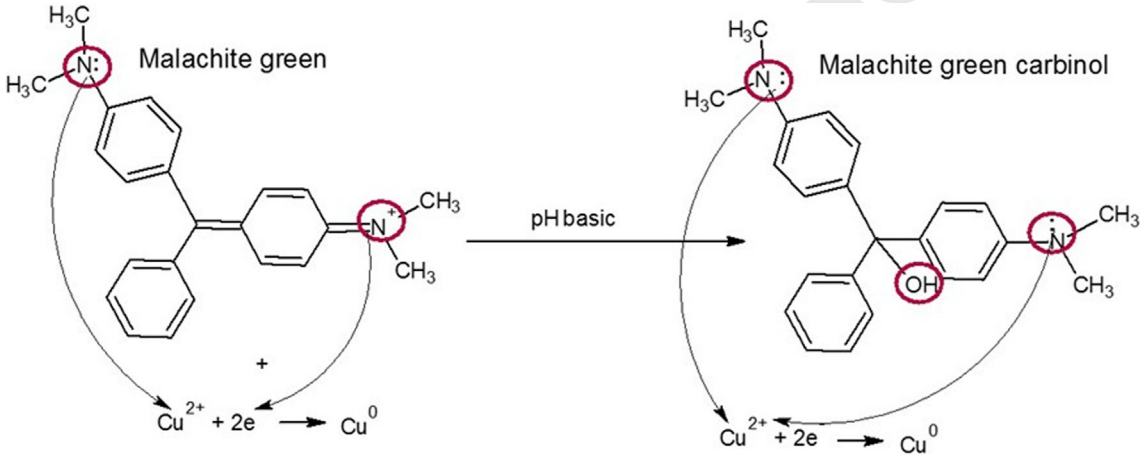

Fig. 11. Mechanism of removal of MG dye with SSW/Fe-Cu nanocomposite.

Table 4
Comparison for MG dye removal with different adsorbent materials.

Adsorbent materials	Method	Initial concentration (mg/L)	Equilibrium time (min)	q_m (mg/g)	Reference
BRC-clay	Adsorption	50–250	100	86.6	[38]
Activated carbon (AC)	Ultrasound assisted	5–25	5	50.3	[39]
CuO-NPs-AC	Ultrasound assisted	–	5	87.7	
Pomegranate peel	Biosorption	30–60	90	31.5	[40]
Carrot stem powder (CSP)	Adsorption	10–50	25	52.6	[41]
Cobalt ferrite silica magnetic nanocomposite	Adsorption	100	40	75.5	[42]
Activated carbon-$CoFe_2O_4$ composites	Mechanical mixing	100	80	89.3	[39]
Chlorella vulgaris biomass	Biosorption	2–10	90	42.3	[43]
SSW/Fe-Cu	Adsorption	30–120	260	88.3	This study
SSB/Fe-Cu	Adsorption		125	63.6	
SSW-TUF/Fe-Cu	Adsorption			267.1	

nanoparticles and dye molecules. The low cost and the ease synthetic methodology of these novel nanocomposites, as well as their high adsorption capacities, making them potential large-scale efficient materials to remove organic dyes.

References

[1] S. Kuppusamy, P. Thavamani, M. Megharaj, K. Venkateswarlu, Y.B. Lee, R. Naidu, Potential of Melaleuca diosmifolia as a novel, non-conventional and low-cost coagulating adsorbent for removing both cationic and anionic dyes, J. Ind. Eng. Chem. 37 (2016) 198–207.
[2] A. Asfaram, M. Ghaedi, S. Hajati, A. Goudarzi, E.A. Dil, Screening, and optimization of highly effective ultrasound-assisted simultaneous adsorption of cationic dyes onto Mn-doped Fe_3O_4-nanoparticle-loaded activated carbon, Ultrason Sonochem. 34 (2017) 1–12.
[3] R. Gopinathan, J. Kanhere, J. Banerjee, Effect of malachite green toxicity on non-target soil organisms, Chemosphere. 120 (2015) 637–644.
[4] A. Jasińska, K. Paraszkiewicz, A. Sip, J. Długoński, Malachite green decolorization by the filamentous fungus Myrothecium roridum-Mechanistic study and process optimization, Bioresour. Technol. 194 (2015) 43–48.
[5] M. Ghaedi, F.N. Azad, K. Dashtian, S. Hajati, A. Goudarzi, M. Soylak, Central composite design and genetic algorithm applied for the optimization of ultrasonic-assisted removal of malachite green by ZnO nanorod-loaded activated carbon, Spectrochim. Acta, Part A 167 (2016) 157–164.
[6] M. Brigante, E. Pecini, M. Avena, Magnetic mesoporous silica for water remediation: Synthesis, characterization and application as adsorbent of molecules and ions of environmental concern, Micropor. Mesopor. Mater. 230 (2016) 1–10.

Please cite this article as: A. Blanco-Flores, H. P. Toledo-Jaldin, A. R. Vilchis-Néstor et al., Metallurgical slag properties as a support material for bimetallic nanoparticles and their use in the removal of malachite green dye, Advanced Powder Technology, https://doi.org/10.1016/j.apt.2020.05.012

[7] R. Kumar, V. Rawat, S. Banerjee, M.A. Sanroman, S.K. Singh, M.C. Chattopadhyaya, Synthesis of bimetallic Fe-Zn nanoparticles and its application towards adsorptive removal of carcinogenic dye malachite green and Congo Red in water, J. Mol Liq. 212 (2015) 227–236.
[8] F. Nekouei, H. Noorizadeh, S. Nekouei, M. Asif, I. Tyagi, S. Agarwal, Vinod K. Gupta, Removal of malachite green from aqueous solutions by cuprous iodide-cupric oxide nanocomposite loaded on activated carbon as a new sorbent for solid phase extraction: Isotherm, kinetics and thermodynamic studies, J. Mol. Liq. 213 (2016) 360–368.
[9] L. Zuo-Peng, W. Ya-Qiong, S. Jian-Peng, W. Mei-Xia, W. Long-Fei, G. Yong, Magnetically recoverable Cu_2O/Fe_3O_4 composite photocatalysts: Fabrication and photocatalytic activity, Chin. Chem Lett. 25 (2014) 287–291.
[10] M. Zienkiewicz-Strzałka, A. Deryło-Marczewska, S. Pikus, Bimetallic systems of mesoporous ordered silica supports and noble metals nanoparticles, Micropor. Mesopor. Mater. 227 (2016) 228–241.
[11] N. Arancibia-Miranda, S.E. Baltazar, A. García, D. Muñoz-Lira, P. Sepúlveda, M. A. Rubio, D. Altbir, Nanoscale zero valent supported by Zeolite and Montmorillonite: Template effect of the removal of lead ion from an aqueous solution, J. Hazard. Mater. 301 (2016) 371–380.
[12] D. Ociński, I. Jacukowicz-Sobala, P. Mazur, J. Raczyk, E. Kociołek-Balawejder, Water treatment residuals containing iron and manganese oxides for arsenic removal from water. Characterization of physicochemical properties and adsorption studies, Chem. Eng. J. 294 (2016) 210–221.
[13] R.N. Hidayah, I. Mohammad, Z. Abdul-Majid, S. Ghoreishiamiri, B. Muhammad, Performance of steel slag and steel sludge in concrete, Const. Build. Mater 104 (2016) 16–24.
[14] Y. Zhang, C. Zhang, X. Zhang, L. Feng, Y. Li, Q. Zhou, Waste activated sludge hydrolysis and acidification: A comparison between sodium hydroxide and steel slag addition, J. Environ. Sci. (2016), https://doi.org/10.1016/j.jes.2016.02.010.
[15] A.S. Vilaplana, V.J. Ferreira, A.M. López-Sabirón, A. Aranda-Usón, C. Lausín-González, C. Berganza-Conde, G. Ferreira, Utilization of Ladle Furnace slag from a steelwork for laboratory scale production of Portland cement, Const. Build. Mater. 94 (2015) 837–843.
[16] A. Blanco-Flores, V. Sánchez-Mendieta, E. Gutiérrez-Segura, A.R. Vilchis-Néstor, R.A. Morales-Luckie, Novel tuffite/Fe-Cu oxides nanocomposite with functionality for dye Removal in aqueous solution, J. Environ. Chem. Eng. 4 (2016) 4472–4484.
[17] L. Bing, T. Biao, M. Zhen, C. Hanchi, L. Hongbo, Physical and chemical properties of steel slag and utilization technology of steel slag at home and abroad, IOP Conf. Series: Earth. Environ. Sci. 242 (2019) 032012.
[18] H. Hu, X. Li, P. Huang, Q. Zhang, W. Yuan, Efficient removal of copper from wastewater by using mechanically activated calcium carbonate, J. Environ. Manage. 203 (2017) 1–7.
[19] J. Eckert, J.C. Holzer, W.L. Johnson, Thermal stability and grain growth behavior of mechanicallly alloyed nanocrystalline Fe-Cu alloys, J. Appl. Phys. 73 (1993) 131–141.
[20] Y.N. Dhoble, S. Ahmed, Review on the innovative uses of steel slag for waste minimization, J. Mater. Cycles Waste Manage. 20 (2018) 1373–1382.
[21] G. López-Téllez, R.A. Morales-Luckie, O.F. Olea-Mejía, V. Sánchez-Mendieta, J. Trujillo-Reyes, V. Varela-Guerrero, A.R. Vilchis-Néstor, Nanoestructuras metálicas: Síntesis, caracterización y aplicaciones, Reverté (2013).
[22] X. Li, Y. Zhao, B. Xi, X. Mao, B. Gong, R. Li, X. Peng, H. Liu, Removal of nitrobenzene by immobilized nanoscale zero-valent iron: Effect of clay support and efficiency optimization, Appl. Surf. Sci. 370 (2016) 260–269.
[23] A. Pourjavadi, A. Abedin-Moghanaki, Ultrafast and efficient removal of cationic dyes using a magnetic nanocomposite based on functionalized cross-linked poly(methylacrylate), React. Funct. Polym. 105 (2016) 95–102.
[24] O. Duman, S. Tunç, B.K. Bozoğlan, T.G. Polat, Removal of triphenylmethane and reactive azo dyes from aqueous solution by magnetic carbon nanotube-k-carrageenan-Fe_3O_4 nanocomposite, J. Alloys Compd. 687 (2016) 370–383.
[25] M. Ghaedi, A. Ansari, M.H. Habibi, A.R. Asghari, Removal of malachite green from aqueous solution by zinc oxide Nanoparticle loaded on activated carbon: Kinetics and isotherm study, J. Ind. Eng. Chem. 20 (2014) 17–28.
[26] A. Asfaram, M. Ghaedi, S. Hajati, A. Goudarzi, Synthesis of magnetic c-Fe2O3-based nanomaterial for ultrasonic assisted dyes adsorption: Modeling and optimization, Ultrason Sonochem. 32 (2016) 418–431.
[27] N. Vaishakh, R. Vinu, Peroxide-assisted microwave activation of pyrolysis char for adsorption of dyes from wastewater, Bioresour. Technol. 216 (2016) 511–519.
[28] K.Y. Foo, B. Hameed, Review. Insights into the modeling of adsorption isotherm systems, Chem. Eng. J. 156 (2010) 2–10.
[29] D. Pathania, A. Sharma, S. Zia-Mahmood, Removal of Congo Red dye from aqueous system using Phoenix dactylifera seeds, J. Mol. Liq. 219 (2016) 359–367.
[30] A. Blanco-Flores, N. Arteaga-Larios, V. Pérez-García, J. Martínez-Gutiérrez, M. Ojeda-Escamilla, I. Rodríguez-Torres, Efficient fluoride removal using Al-Cu oxide nanoparticles supported on steel slag industrial waste solid, Environ. Sci. Pollut. Res. 25 (2018) 6414–6428.
[31] S. Venkata Mohan, S.V. Ramanaiah, B. Rajkumar, P.N. Sarma, Removal of fluoride from aqueous phase by biosorption onto algalbiosorbent Spirogyra sp.-IO2: Sorption mechanism elucidation, J. Hazard. Mater. 141 (2007) 465–474.
[32] J.F. Moulder, M.F. Stickle, PE. Sobol, K.D. Bomben, Handbook of X-Ray Photoelectron Spectroscopy. Publishing by: Perkin-Elmer, EU, ISBN: 0-9627026-2-5, (1992).
[33] T. Ghodselahi, M.A. Vesaghi, A. Shafiekhani, A. Baghizadeh, M. Lameii, XPS study of the Cu@Cu_2O core-shell nanoparticles, Appl. Surf. Sci. 255 (2008) 2730–2734.
[34] H. Mao, X. Qiu, D. Li, Y. Lin, X. Liu, J. Li, Cu (I) Modification during γ-Fe2O nanoparticles synthesis and subsequent characterization, J. Chem. (2015) 1–9, http://dx.doi.org/10.1155/2015/573657.
[35] S. Edebali, E. Pehlivan, Evaluation of chelate and cation exchange resins to remove copper ions, Powder Technol. 301 (2016) 520–525.
[36] A. Blanco-Flores, E. Gutiérrez-Segura, V. Sánchez-Mendieta, A.R. Vilchis-Néstor, Removal of malachite green dye from aqueous solution through inexpensive and easily available tuffite, bentonite and vitreous tuff minerals, Rev. Latinoamericana de Recursos Nat. 12 (2016) 1–17.
[37] A.A. Cikmit, T. Tsuchida, R. Hashimoto, H. Honda, G. Kang, K. Sogawa, Expansion characteristic of steel slag mixed with soft clay, Constr. Build. Mater. 227 (2019) 116799.
[38] R. Elmoubarki, F.Z. Mahjoubi, H. Tounsadi, J. Moustadraf, M. Abdennouri, A. Zouhri, A. El Albani, N. Barka, Adsorption of textile dyes on raw and decanted Moroccan clays: Kinetics, equilibrium and thermodynamics, Water Resour. Ind. 9 (2015) 16–29.
[39] E.A. Dil, M. Ghaedi, A. Asfaram, S. Hajati, A. Goudarzi, Preparation of nanomaterials for the ultrasound-enhanced removal of Pb^{2+} ions and malachite green dye: Chemometric optimization and modeling, Ultrason. Sonochem. 34 (2017) 677–691.
[40] F. Gündüz, B. Bayrak, Biosorption of malachite green from an aqueous solution using pomegranate peel: Equilibrium modelling, kinetic and thermodynamic studies, J. Mol. Liq. 243 (2017) 790–798.
[41] A. Kumar, N. Gupta, M.C. Chattopadhyaya, Removal of cationic methylene blue and malachite green dyes from aqueous solution by waste materials of Daucus carota, J. Saudi Chem. Soc. 18 (2014) 200–207.
[42] M. Amiri, M. Salavati-Niasari, A. Akbari, T. Gholami, Removal of malachite green (a toxic dye) from water by cobalt ferrite silica magnetic nanocomposite: Herbal and green sol-gel autocombustion synthesis, Int. J. Hydrog. Energy. 42 (2017) 24846–24860.
[43] M. Kousha, O. Farhadian, S. Dorafshan, N.M. Soofiani, A. Bhatnagar, Optimization of malachite green biosorption by green microalgae-Scenedesmus quadricauda and Chlorella vulgaris: Application of response surface methodology, J. Taiwan Institute Chem. Eng. 44 (2013) 291–294.

Please cite this article as: A. Blanco-Flores, H. P. Toledo-Jaldin, A. R. Vilchis-Néstor et al., Metallurgical slag properties as a support material for bimetallic nanoparticles and their use in the removal of malachite green dye, Advanced Powder Technology, https://doi.org/10.1016/j.apt.2020.05.012